Published in final edited form as:
Neuroimage. 2008 March 1; 40(1): 43–52. doi:10.1016/j.neuroimage.2007.11.011.

Kinetic Analysis in Healthy Humans of a Novel Positron Emission Tomography Radioligand to Image the Peripheral Benzodiazepine Receptor, a Potential Biomarker for Inflammation

Masahiro Fujita[1], **Masao Imaizumi**[1], **Sami S. Zoghbi**[1], **Yota Fujimura**[1], **Amanda G. Farris**[1], **Tetsuya Suhara**[2], **Jinsoo Hong**[1], **Victor W. Pike**[1], and **Robert B. Innis**[1]

1*Molecular Imaging Branch, National Institute of Mental Health, National Institutes of Health, Bethesda, MD, USA*

2*Molecular Neuroimaging Group, Molecular Imaging Center, National Institute of Radiological Sciences, Chiba, Japan*

Abstract

The peripheral benzodiazepine receptor (PBR) is upregulated on activated microglia and macrophages and thereby is a useful biomarker of inflammation. We developed a novel PET radioligand, [^{11}C]PBR28, that was able to image and quantify PBRs in healthy monkeys and in a rat model of stroke. The objective of this study was to evaluate the ability of [^{11}C]PBR28 to quantify PBRs in brain of healthy human subjects. Twelve subjects had PET scans of 120 to 180 min duration as well as serial sampling of arterial plasma to measure the concentration of unchanged parent radioligand. One- and two-tissue compartmental analyses were performed. To obtain stable estimates of distribution volume, which is a summation of B_{max}/K_D and nondisplaceable activity, 90 min of brain imaging was required. Distribution volumes in human were only ~5% of those in monkey. This comparatively low amount of receptor binding required a two- rather than a one-compartment model, suggesting that nonspecific binding was a sizeable percentage compared to specific binding. The time-activity curves in two of the twelve subjects appeared as if they had no PBR binding - i.e., rapid peak of uptake and fast washout from brain. The cause(s) of these unusual findings are unknown, but both subjects were also found to lack binding to PBRs in peripheral organs such as lung and kidney. In conclusion, with the exception of those subjects who appeared to have no PBR binding, [^{11}C]PBR28 is a promising ligand to quantify PBRs and localize inflammation associated with increased densities of PBRs.

Keywords

Compartmental analysis; microglia; distribution volume; Monte-Carlo simulation; aryloxyanilide

Address correspondence and reprint requests: Masahiro Fujita, MD, PhD, Molecular Imaging Branch, National Institute of Mental Health, Building 31, Room B2B37, 31 Center Drive, MSC-2035, Bethesda, MD 20892-2035, USA. FAX: +1-301-480-3610, TEL: +1-301-451-8898, E-MAIL: FujitaM@intra.nimh.nih.gov.

INTRODUCTION

The peripheral benzodiazepine receptor (PBR) is a mitochondrial protein that is highly expressed in phagocytic inflammatory cells, namely macrophages in the periphery and activated microglia in the central nervous system (Papadopoulos et al., 2006; Zavala et al., 1984). Both *in vitro* and *in vivo* imaging of PBRs can localize and quantify inflammation in tissues (Venneti et al., 2006). For the past two decades, [^{3}H]PK 11195 has been used for *in vitro* studies (e.g., binding to homogenates or sections of tissues), and the PET radioligand [^{11}C]PK 11195 has been used for *in vivo* imaging (Venneti et al., 2006). [^{3}H]PK 11195 is useful as an *in vitro* radioligand and has a high ratio of specific to nonspecific binding, in part because much of the nonspecific binding can be washed away from tissue homogenates or sections. Such washing is not possible for *in vivo* imaging, and [^{11}C]PK 11195 has relatively low ratios of specific to nonspecific binding. For example, by using reference tissue models, Kropholler et al. have reported that the ratio of specific to nonspecific binding of the active enantiomer (*R*) of [^{11}C]PK 11195 in human brain is only about 0.2 - 0.5 (Kropholler et al., 2006).

A new class of ^{11}C- and ^{18}F-labeled radioligands with an aryloxyanilide structure has been developed for *in vivo* imaging of PBR with PET (Okuyama et al., 1999). These radioligands have 4 to 18 times greater affinity for PBRs than PK 11195 and have higher levels of brain uptake (Zhang et al., 2003). Among this class of ligands, [^{11}C]DAA1106 and [^{18}F] FEDAA1106 have been studied in monkeys and demonstrate high brain uptake and high ratios of specific to nonspecific binding (Maeda et al., 2004; Zhang et al., 2004). Studies in human with these ligands show high brain uptake, but displacement studies have not been performed to measure definitively the percentage of specific binding in human brain (Fujimura et al., 2006; Ikoma et al., 2007). Furthermore, [^{11}C]DAA1106 has been directly compared with [^{11}C](*R*)-PK11195 in rats under baseline conditions and after inflammation had been induced with neurotoxins (Venneti et al., 2007a; Venneti et al., 2007b). The radioligand with an aryloxyanilide structure, [^{11}C]DAA1106, was superior to that with an isoquinoline structure, [^{11}C](*R*)-PK11195, in terms of higher brain uptake and retention in areas with inflammation.

We recently developed additional ^{11}C- and ^{18}F-labeled analogs with an aryloxyanilide structure, and some showed promising results in animals. One of these compounds is [^{11}C] PBR28 ([*O-methyl*-^{11}C]*N*-acetyl-*N*-(2-methoxybenzyl)-2-phenoxy-5-pyridinamine). The affinity of PBR28 for peripheral benzodiazepine receptors (K_I, inhibition constant = 0.7 - 2.5 nM in rat, monkey and human) is 2 - 5 fold greater than that of PK 11195, and the lipophilicity of PBR28 is ~100 fold lower than that of PK 11195 (Briard et al., in press). The relatively high affinity and low lipophilicity likely contribute to the high *in vivo* specific signal of [^{11}C]PBR28. For example, more than 90% of uptake into monkey brain can be displaced by nonradioactive PBR ligands, and such displacement is the pharmacological definition of specific binding (Imaizumi et al., In press). Because of the promising imaging results in monkeys, we extended the use of this radioligand to human subjects. Based on whole body biodistribution in healthy subjects, the effective dose of [^{11}C]PBR28 is 6.6 μSv/MBq, similar to that of other ^{11}C-labeled ligands (Brown et al., In press).

Having confirmed the radiation safety of [^{11}C]PBR28, we sought in the current study to evaluate the ability of this radioligand to quantify PBRs in human brain. Binding in brain was quantified with compartmental modeling using serial brain images and concurrent measurements of unchanged parent radioligand in arterial plasma.

MATERIALS AND METHODS

Radiopharmaceutical preparation

[^{11}C]PBR28 was prepared by the ^{11}C-methylation of its desmethyl analogue with [^{11}C] iodomethane, itself prepared from cyclotron-produced [^{11}C]carbon dioxide, and purified with reverse phase HPLC. Preparations were conducted according to our exploratory Investigational New Drug Application #73,935, submitted to the US Food and Drug Administration, and a copy of which is available at: http://kidb.bioc.cwru.edu/snidd/. The radioligand was obtained in high radiochemical purity (> 99%).

Human subjects

Twelve healthy volunteers participated: 1 female and 11 males, 25 ± 5 years of age, 81 ± 15 kg body weight (these and subsequent numerical data are expressed as mean ± SD). All subjects were free of current medical and psychiatric illness based on history, physical examination, electrocardiogram, urinalysis including drug screening, and blood tests (complete blood count, serum chemistries, thyroid function test, and antibody screening for syphilis, HIV, and hepatitis B). Approximately 24 h after the PET scan, subjects returned to repeat urinalysis and blood tests.

PET scans

We used two PET cameras: High Resolution Research Tomograph (HRRT; Siemens/CPS, Knoxville, TN, USA) and GE Advance (GE Healthcare, Waukesha, WI, USA). HRRT and GE Advance cameras have reconstructed resolution of 2.5 mm and 7.5 mm full-width half-maximum in all directions in 3D mode, respectively. The HRRT was used only in the first scan to see if the human brain contained a small region with high levels of binding, such as choroid plexus in monkeys (Imaizumi et al., In press). As expected from previous postmortem studies (Cymerman et al., 1986; Doble et al., 1987), binding of [^{11}C]PBR28 was fairly uniform in human brain, and we saw no small region with high levels of binding. Therefore, all subsequent scans were performed using the GE Advance. The results from both cameras were combined for statistical analysis because the results from the HRRT, including estimates of the rate constants, were well within the range of those from the GE Advance.

After injection of 650 ± 92 MBq (specific activity at time of injection of 170 ± 81 GBq/μmol) of [^{11}C]PBR28, PET scans were acquired for 120 to 180 min in 33 to 45 frames with scan duration ranging from 30 s to 5 min. Six subjects completed scans with durations of at least 150 min.

Magnetic resonance imaging

To identify brain regions, magnetic resonance imaging (MRI) scans of 1.2-mm contiguous slices were obtained with a 1.5-T GE Signa device. Three sets of axial images were acquired parallel to the anterior-commissure-posterior commissure line with Spoiled Gradient Recalled (SPGR) sequence with TR=12.4 ms, TE=5.3 ms, flip angle = 20°, and matrix=256×256.

Measurement of [^{11}C]PBR28 in plasma

Blood samples (1.0 mL each) were drawn from the radial artery at 15 s intervals until 150 s, followed by 3-mL samples at 3, 4, 6, 8, 10, 15, 20, 30, 40, 50, 60, 75, 90, and 120 min. The plasma time-activity curve was corrected with the fraction of unchanged radioligand, as previously described including our monkey study of [^{11}C]PBR28 (Zoghbi et al., 2006) (Imaizumi et al., In press). In all scans, plasma free fraction of [^{11}C]PBR28 was measured as described previously (Carson et al., 1993).

Image analysis

Image and kinetic analyses were performed using PMOD 2.80 (pixel-wise modeling software; PMOD Technologies Ltd., Adliswil, Switzerland) (Burger et al., 1998). HRRT data were reconstructed on a 256×256 matrix with a pixel size of 1.22×1.22×1.23 mm in the x, y, and z axis, respectively. GE Advance data were reconstructed on a 128×128 matrix with a pixel size of 2.0×2.0×4.25 mm in the x, y, and z axis, respectively. Correction for attenuation and scattered radiation were performed for all data. Head motion during the HRRT scan was corrected using Polaris Vicra Optical Tracking System (NDI, Waterloo, Ontario, Canada). All GE images of each subject were coregistered to each other using Statistical Parametric Mapping 5 (SPM 5; Wellcome Department of Cognitive Neurology, London, U.K.). PET images during the first 15 min were averaged to create images with good delineation of cerebral cortices. Using SPM 5, for each subject, three SPGR images were realigned and an average image was created to improve signal-to-noise ratio. The average MR image was coregistered to the average PET image, and both MR and all PET images were spatially normalized to a standard anatomic orientation (Montreal Neurological Institute space) by obtaining parameters from the MR image. Volumes of interest were placed on average of spatially normalized MR images overlying the thalamus (12.6 cm^3), caudate (5.6 cm^3), putamen (6.5 cm^3), cerebellum (51.2 cm^3), pons (10.6 cm^3); and frontal (27.2 cm^3), parietal (26.6 cm^3), temporal (25.0 cm^3), and occipital cortices (31.2 cm^3).

Estimation of distribution volume with metabolite-corrected arterial input function

Time-activity data were analyzed with both one- and two-tissue compartment models, using the radiometabolite-corrected plasma input function. The input function was calculated as linear interpolation of the concentrations of [^{11}C]PBR28 before the peak, and a tri-exponential fit of concentrations after the peak. [^{11}C]PBR28 was used as the sole input function, because HPLC analysis in rat showed that the vast majority, namely 94%, of brain activity was [^{11}C]PBR28 at 30 min after injection (Briard et al., in press). Rate constants (K_1, k_2, k_3, and k_4) in standard one- and two-tissue compartment models (Innis et al., 2007) were estimated with weighted least squares and the Marquardt optimizer. Brain data of each frame were weighted relative to other frames by assuming that the standard deviation of the data was proportional to the inverse square root of noise equivalent counts. Each frame was weighted with inverse square of the standard deviation. Each model configuration was implemented to account for the contribution from activity in the cerebral blood volume. In each model, by using measured whole blood activity, cerebral blood volume was assumed to be 5% of brain volume. Delay between arrival of [^{11}C]PBR28 in radial artery and brain was estimated by fitting the whole brain excluding the areas of mostly white matter.

Two-compartmental fitting was performed in two ways, without constraint and by fixing K_1/k_2 to the value obtained in the whole brain excluding the areas of mostly white matter. The purpose of the constraint is to estimate k_3 with better accuracy to perform Monte Carlo simulations by changing k_3.

We followed the recently proposed consensus nomenclature for reversibly binding radioligands (Innis et al., 2007), where V_T is total distribution volume, including specific and nondisplaceable uptake.

Minimal time required to estimate distribution volume

To investigate the effect of reducing the duration of the scan on measurement of V_T, kinetic analyses were performed after deleting increasing segments of the complete study. Since all subjects were scanned for at least 120 min, we analyzed brain data of all subjects from 0 - 30 min to 0 - 120 min, with 10 min increments. Since six subjects were imaged for at least 150 min, we similarly analyzed data from these subjects from 0 - 30 min to 0 - 150 min.

Monte Carlo simulations

Inflammation can be associated with several fold increased densities of PBRs (Venneti et al., 2006). We performed Monte Carlo simulations to investigate if such large increases in receptor binding could be measured accurately *in vivo* with [^{11}C]PBR28. Increases in the binding were simulated by increasing k_3 obtained from the two-tissue compartment model with a fixed value of K_1/k_2. Average input function expressed as % standard uptake value (SUV) was used as the input. Because thalamus showed the largest V_T, average rate constants of this region ($K_1 = 0.12$ mL • cm^{-3} min^{-1}, $k_2 = 0.11$ min^{-1}, $k_3 = 0.069$ min^{-1}, and $k_4 = 0.023$ min^{-1}) were used. Simulations were performed for increases in k_3 by 2, 3, 4, 5, 6, 7, 8, 9, and 10-fold. Brain time-activity curves were generated for each value of k_3, and Gaussian noise added. We selected a noise level such that SD of Gaussian distribution was equal to 7.5% of the mean activity at each time point. This SD value of 7.5% was selected because it gave a reproducibility of 3.1% for the baseline data, which was close but slightly greater than the actual identifiability of observed brain data (Table 1). One thousand runs were performed for each set of rate constants.

The accuracy of estimating V_T was evaluated in terms of bias (percentage difference between observed and actual values) and reproducibility (COV = SD/mean) of V_T.

Statistical analysis

Goodness-of-fit by nonlinear least squares analysis was evaluated using the Akaike Information Criterion (AIC) (Akaike, 1974) and model selection criterion (MSC). MSC is a modification of the AIC (see Appendix) and was proposed by Micromath Scientific Software (Salt Lake City, Utah, USA) and implemented in their program, "Scientist." The most appropriate model is that with the *smallest* AIC and the *largest* MSC value. Although AIC values are affected by the unit or the concentration of the brain activity, MSC values are independent of these parameters by having errors of fitting in both the numerator and the denominator. Therefore, MSC can be used to compare goodness-of-fit among different scans.

Goodness-of-fit by the compartment models was compared with *F* statistics (Hawkins et al., 1986). A value of $P < 0.05$ was considered significant for *F* statistics.

The identifiability (%) of the kinetic variables was expressed as the standard error of non-linear least squares estimation. The standard error is calculated from the diagonal of the covariance matrix (Carson, 1986) and expressed as a percentage of the rate constant. identifiability (%) of V_T was calculated from the covariance matrix using the generalized form of error propagation equation (Bevington and Robinson, 2003), where correlations among parameters (K_1, and k_2, or K_1, k_2, k_3, and k_4) were taken into account. Greater numbers in identifiability (%) indicate poorer identifiability.

RESULTS

Pharmacological effects

Injection of [^{11}C]PBR28 caused no pharmacological effects, based on patient reports, ECG, blood pressure, pulse, and respiration rate after radioligand administration. In addition, no effects were noted in any of the blood and urine tests acquired about 24 h after radioligand injection. The injected mass dose of PBR28 was 4.9 ± 2.6 nmol (n = 13 injections in 12 subjects).

Brain images: binders

After injection of [^{11}C]PBR28, 10 of 12 subjects showed moderate levels of activity in brain that washed out gradually. The peak uptake occurred at 5 min and was ~200% SUV (Fig. 1A). Brain activity decreased to 50% of the peak by 70 min and to 40% of peak by 120 min. As

expected from known distribution of PBRs in human brain (Cymerman et al., 1986;Doble et al., 1987), the distribution of activity was widespread and fairly uniform in gray matter of cerebral cortices and cerebellum, basal ganglia, and thalamus (Fig. 1B). A brain region without PBRs can be used as a reference region in kinetic analysis. However, there appeared to be no such a region.

Brain images: nonbinders

Two of 12 subjects had a strikingly different time course of radioactivity in brain, including markedly faster washout. Both subjects were 25 year old males; one was Euro-American and one was Hispanic. In comparison to the 10 other subjects, a total of three scans of these two unusual subjects showed a higher peak of 216%, 234%, and 341% SUV at an earlier time (2 min instead of 5 min for the other 10 subjects) (Fig. 1C). Activity washed quickly from brain and was at half of the peak concentration within only 6-7 min, compared to the other 10 subjects. In addition, brain activity remained almost constant after ~20 min.

One of the two subjects reported taking ibuprofen (1000 mg per day for several days/weeks) prior to the first scan. To test whether the ibuprofen may have blocked radioligand binding in brain, after ~100 days off ibuprofen and 114 days after the first PET scan, we repeated the brain scan in this subject. The second scan was almost identical to the first in terms of peak uptake and washout rate.

Plasma analysis: binders

The concentration of [^{11}C]PBR28 peaked at ~90 s and rapidly declined thereafter following a curve that was well fit as a triexponential function. The peak concentration was ~1,400% SUV on average and decreased to 50% of the peak at 2 min and to 10% at 6 min (Fig. 2A). Tri-exponential fitting converged in all scans with 5.8% average errors of fitting and showed half lives of 0.34, 4.3, and 42 min. Calculated as the partial area under the concentration vs. time curve, these three half lives accounted for 14%, 33%, and 53% of the area under the curve from the peak to infinity.

A radiometabolite of [^{11}C]PBR28 appeared quickly in plasma and later became the predominant component of plasma radioactivity. The radiometabolite eluted earlier than [^{11}C]PBR28 on reversed phase HPLC (Fig. 2B and 2C) and therefore appears less lipophilic than [^{11}C]PBR28. The fraction of [^{11}C]PBR28, expressed as a percentage of total plasma radioactivity, declined gradually and reached 50% at 15 min (Fig. 2D). The concentration of the radiometabolite significantly increased during the course of the study and was 97% of total plasma radioactivity at 120 min. The net effect of declining concentration of [^{11}C]PBR28 and increasing concentration of radiometabolite was that the total concentration of radioactivity in plasma declined by only 6% from 30 to 120 min (Fig. 2A). Finally, the plasma free fraction of [^{11}C]PBR28 was 3.3 ± 0.5%.

Plasma analysis: nonbinders

The plasma concentration of [^{11}C]PBR28 in the two nonbinders tended to be higher than that of the 10 other subjects. For example, the peak concentrations in the nonbinders were 2,100%, 2,200%, and 4,500% SUV, whereas the average in the other 10 subjects was 1,400%. Nevertheless, the time course of plasma concentrations of [^{11}C]PBR28 in nonbinders was similar to that of other subjects. Tri-exponential fitting converged in all scans with 4.3% average errors of fitting. The average half-lives (and % contribution to the entire area under the curve) were 0.51 min (17%), 4.0 min (14%), and 31 min (69%). Finally, the average plasma free fraction was 2.7% in the nonbinders, compared to 3.3% in the binders. Thus, the trend of higher peak brain activity in the nonbinders may have been caused by higher peak plasma

concentrations of [^{11}C]PBR28. However, the rapid washout of radioactivity from brain of nonbinders was not explained by the decline of the plasma concentration of [^{11}C]PBR28.

Kinetic analysis: binders

The unconstrained two-tissue compartment model provided significantly better fit than the one-tissue compartment model, consistent with the presence of significant amounts of both specific and nonspecific binding in human brain. Because all 10 subjects had a scan of at least 2 h duration, results from 2 h data are reported here. The one-tissue compartment model estimated K_1 and k_2 with good average identifiability (%) of 3.8% and 6.8%, respectively (Table 2). identifiability of V_T was 4.2%. However, the fitting deviated from the measured brain data (Fig. 1A) and had high AIC score of 187 and low MSC of 1.6. The unconstrained two compartment model fitted the data better than the one-compartment model with low AIC of 102 and high MSC of 4.2. *F*-test showed that the two-compartment model gave statistically better fitting in all regions of all subjects. The superiority of two- over one-compartment model was also supported by Logan plots applied as a supplementary analysis, which showed linear fitting not from time 0 but from ~28 min in real time (data not shown).

The unconstrained two compartment model gave average rate constants of $K_1 = 0.13$ mL • cm^{-3} · min^{-1}, $k_2 = 0.11$ min^{-1}, $k_3 = 0.062$ min^{-1}, and $k_4 = 0.024$ min^{-1}, resulting in $BP_{ND} = 2.6$ and $V_T = 4.0$ mL • cm^{-3} (Table 1). Compared to the one-compartment model, the two-compartment model estimated K_1 with similar identifiability of 3.3%, while k_2, k_3, and k_4 were not well identified and had identifiability of 10% or greater. Nevertheless, the two-compartment model well identified V_T and had an average identifiability of 3.9%. Therefore, the unconstrained two-compartment model well described the kinetics of [^{11}C]PBR28. An alternative measure of receptor binding, BP_{ND} was not identified so well as V_T and showed an average identifiability of 9.2%. In addition to parameters directly describing ligand binding, both V_T and BP_{ND} include V_{ND}, which is not relevant to binding. Because V_T was identified better, V_T was used as the measure of ligand binding for further analyses.

Kinetic analysis: nonbinders

Distribution volume in the two nonbinders could not be estimated with reasonable identifiability using either the one- or the unconstrained two-compartment model. Because of almost constant brain activity after ~20 min, the dissociation rate constant k_4 could not be identified, and the two-compartment model did not converge. The one-compartmental fitting significantly deviated from the observed data (Fig. 1C) and had AIC and MSC scores of 172 - 176 and 0.1 - - (negative) 0.5, respectively. Therefore, V_T could not be measured accurately in the nonbinders.

Minimal scan time required to estimate distribution volume

To determine the minimal scanning time required to obtain stable values of distribution volume, we increasingly truncated the brain data from its complete duration of 120 or 150 min to only the initial 30 min. Data of only the binders were analyzed, since V_T of the nonbinders could not be measured accurately. We used the unconstrained two-compartment model. All 10 binders were imaged for at least 120 min. For these 10 subjects, V_T determined with data from the initial 90 min was only 6% less than that determined from the entire 120 min (Fig. 3). Six of the ten subjects were imaged for at least 150 min. For these six subjects, V_T determined with data from the initial 90 min was still only 11% less than that determined from the entire 150 min. Thus, V_T was stably estimated with about 90 min of image acquisition. Furthermore, V_T had high identifiably whether determined with acquisitions of 90 min (3.2%) or 120 min (3.9%). Nevertheless, V_T was not completely stable after 90 min, since it increased by 11% from 90 to 150 min. This relatively small and gradual increase could have been caused by the

accumulation of radiometabolites in brain. The underestimation of compartmental fitting (Fig. 1A) might have also been caused by radiometabolites in brain.

Simulations of increased receptor density

[^{11}C]PBR28 could be used to measure areas with increased density of PBRs associated with inflammation. To assess the ability of [^{11}C]PBR28 to quantify such an increase, we simulated conditions of increased receptor density. That is, we increased the value of k_3, which is proportional to receptor density, but did not change other rate constants. For the simulations, we used the constrained two-compartment model by fixing K_1/k_2, which tended to improve identifiability of rate constants with 3.3% (unconstrained)/1.8 (constrained), 13.2/4.6, 10.5/9.4 for K_1, k_3, and k_4, respectively, although both unconstrained and constrained models identified the major outcome variable, V_T, with equal identifiability (*i.e.*, 3.9%). Increases in k_3 showed little effect on the value of V_T, and bias from the theoretical value was within ± 1.5% for all levels of k_3. However, increases in k_3 almost linearly made identifiability poorer (greater numbers in %identifiability) reaching to ~10% with a six-fold increase in k_3 and nearly 20% with a 10-fold increase (Fig. 4). That is, although not biased, the estimation of V_T was less reproducible with increased receptor densities - i.e., the precision of V_T was decreased with increased receptor densities.

DISCUSSION

[^{11}C]PBR28 had generally promising imaging characteristics, including peak concentrations in brain (~200% SUV) that were moderate in healthy subjects who presumably had no inflammation in brain. Brain uptake could be quantified with a two-tissue compartment model as distribution volume, which provided relatively stable values after about 90 min of imaging. Nevertheless, the estimates of distribution continued to increase in the later portion of longer scan durations: ~11% from 90 to 150 min. This increasing estimate of distribution volume was consistent with a small amount of radiometabolites in brain. Radiochromatography of plasma showed only one radiometabolite. Although this radiometabolite had lower lipophilicity than [^{11}C]PBR28 and would presumably have less entry to brain, the radiometabolite accounted for 97% of plasma radioactivity by 120 min. Two of the 12 healthy subjects had a time course of brain activity that would be mimicked by the absence of PBRs or by blockade of PBRs. The reason(s) for the unusual results in these two subjects are not known.

Comparison of [^{11}C]PBR28 imaging in humans and monkeys

The current results of [^{11}C]PBR28 imaging in humans were different from our prior studies in rhesus monkey in two ways, which may be related. First, receptor binding in monkey brain was much higher (~20 fold) than in human brain. Second, modeling was adequately performed with one-tissue compartment in monkeys but required two-tissue compartments in humans. That is, the human data was consistent with a sizeable proportion of brain activity being nonspecific binding.

The binding of [^{11}C]PBR28 in brain, estimated as distribution volume, was about 20 fold higher in monkey than in human. That is, V_T was ~100 - 150 mL • cm^{-3} in monkey brain and only ~4 mL • cm^{-3} in human brain. Since only radioligand that is not bound to plasma proteins is able to cross the blood-brain barrier, a more accurate comparison of binding would correct for free fraction f_P. With this correction, V_T/f_P was ~2,000 - 3,000 mL • cm^{-3} (f_P = 5.6%) in monkey brain and only ~120 mL • cm^{-3} (f_P = 3.3%) in human brain. Although differences in PBR density between rhesus monkey and human are reported in only a limited number of regions (Cymerman et al., 1986; Pazos et al., 1986), the relative receptor binding of [^{11}C]PBR28 in our studies was consistent with these *in vitro* reports.

A second difference between these two species was that modeling of [^{11}C]PBR28 required only one-tissue compartment in monkeys but two tissue compartments in humans. This difference was likely caused by the fact that the vast majority (>90%) of brain uptake in monkey is specific and can be blocked by nonradioactive PBR ligands. We did not perform such blockade in human subjects, but we know that total brain uptake (i.e., specific plus nondisplaceable) in humans is 1/20th that in monkey. In monkey, nondisplaceable distribution volume adjusted by plasma free fraction (V_{ND} / f_P) was ~30 mL • cm^{-3}. If nondisplaceable uptake is similar in both species, then 25% of total brain uptake in humans is nondisplaceable (i.e., 30 / 120 = 25%). In summary, a greater percentage of nondisplaceable uptake relative to specific binding in human than in monkey brain could have caused a two-compartment model to be significantly better than a one-compartment model in human because nondisplaceable and specific binding compartments were more distinguishable.

Simulations of increased binding

An area with high density of glia or significant inflammation may have several fold increased density of PBRs (Venneti et al., 2006). Therefore, in addition to measuring low density of receptors found in healthy human brain, a useful PET radioligand must also be able to measure areas of increased binding. A common difficulty with such measurements is that the densely packed receptors delay the washout of radioligand by binding and rebinding, and the delay may extend beyond the useful half-life of the radionuclide. We simulated up to 10-fold increased receptor density and found that the major outcome measure, distribution volume (V_T), was estimated without bias but with lower reproducibility (*i.e.*, less precision). Although this simulation suggests that [^{11}C]PBR28 can provide reasonably accurate measurements of V_T with increases of up to about five fold, real studies in patients will be required to assess this simulated result and the impact of other possible changes caused by inflammation such as increase in permeability of blood brain barrier. Furthermore, if increased densities of PBR are difficult to measure with [^{11}C]PBR28, a longer-lived ^{18}F-labeled radioligand, such as [^{18}F] PBR06, may be advantageous (Imaizumi et al., 2007a).

Nonbinders

Two of the 12 healthy subjects had time courses of brain activity that would be mimicked by the absence of PBRs or by blockade of PBRs. That is, the peak plasma concentration was higher, the peak brain radioactivity was higher, and the washout of radioactivity from brain was faster in these two unusual subjects than in the other ten subjects. We found similar results in monkeys who received receptor-blocking doses of nonradioactive PBR ligand prior to [^{11}C]PBR28 injection (Brown et al., In press; Imaizumi et al., In press). Whole body imaging in a monkey showed blockade of binding to peripheral organs, such as kidney, lung, and spleen, which have high densities of PBRs. This blockade of distribution of radioligand to peripheral organs caused higher concentrations of [^{11}C]PBR28 in plasma and consequently higher peak radioactivity in brain. Since receptors in brain were also unavailable to bind radioligand, the brain activity washed out much faster in monkeys after preblockade than under baseline conditions. Thus, these two subjects showed time courses of brain activity that were similar to those in monkeys that had no receptors available for binding. Furthermore, we performed whole body imaging in both of these subjects, and they showed negligible binding to kidneys, lungs, and spleen (results of one of these subjects were included in (Brown et al., In press)). Thus, these two subjects appeared to lack the binding site of [^{11}C]PBR28 or lack PBR receptors in both brain and periphery.

The cause(s) of the unusual time course of brain activity in these two subjects are unknown but are likely not medications. One of the two subjects was taking modest doses of ibuprofen (1000 mg/day), but the brain imaging results were replicated after discontinuing this medication for ~100 days. This subject was taking no medication other than ibuprofen, and

the second subject was taking none at all. Furthermore, the urine of both subjects was negative for common drugs of abuse. To explore possible causes of the unusual brain uptake, we plan to examine polymorphisms of the PBR gene including those reported (Kurumaji et al., 2000) and also perform *in vitro* binding to PBRs located on white blood cells.

What is the incidence of this unusual finding in healthy subjects? Since the time of this study, we have performed whole body and/or brain imaging with [^{11}C]PBR28 in a total of 29 healthy subjects. Four subjects including two reported here showed time activity curves that suggest no available PBRs in brain and/or periphery. Thus, the incidence to date is 4 / 29 or 14%.

Comparison of [^{11}C]PBR28 and [^{11}C](*R*)-PK 11195

Is our new radioligand, [^{11}C]PBR28, better than [^{11}C](*R*)-PK 11195, which has been studied for more than a decade? Although many reports have been published on [^{11}C](*R*)-PK 11195, and we have performed extensive evaluations of [^{11}C]PBR28 in animals (Imaizumi et al., In press; Imaizumi et al., 2007b) and healthy human subjects ((Brown et al., In press) and current study), we do not know the answer to this question. The problems with making comparisons are that the two radioligands have been studied under somewhat different conditions and [^{11}C]PBR28 has not yet been studied in patients with neuroinflammation. Nevertheless, some limited comparisons can be made.

The total brain uptake of [^{11}C]PBR28 appears to be higher than that of [^{11}C](*R*)-PK 11195 but the percentage of specific binding is difficult to compare. After an initial sharp peak, the brain uptake of [^{11}C](*R*)-PK 11195 appears to be ~100% SUV (Cagnin et al., 2001; Kropholler et al., 2005). In contrast, the brain uptake of [^{11}C]PBR28 was ~200% in healthy subjects (Fig. 1A). Of this total brain uptake, the percentage that is specific is critically important, since we seek to measure specific (or receptor-bound) radioligand. Unfortunately, blockade studies using nonradioactive ligands have been performed in different species for the two radioligands. We found that more than 90% of brain uptake of [^{11}C]PBR28 in monkey brain was specific - i.e., blocked by pharmacological doses of nonradioactive DAA1106 (Imaizumi et al., In press). Similar studies are not reported for [^{11}C](*R*)-PK 11195, but one displacement study was performed in a human subject with a glioma using racemic [^{11}C]PK 11195 (Pappata et al., 1991). In this case, visual inspection of the time-activity curve shows that about 1/3 of activity in the glioma was displaced within 10 min of injection PK 11195 (57 μmol i.v.). Studies with identical design in the same species will be required to compare accurately the two radioligands, [^{11}C](*R*)-PK 11195 and [^{11}C]PBR28. Furthermore, the clinical utility of the two radioligands will likely require side-by-side comparisons in patients with neuroinflammation.

The existence of nonbinders for [^{11}C]PBR28 is a clear disadvantage of this radioligand. To our knowledge, nonbinders have not been reported for [^{11}C](*R*)-PK 11195. Nevertheless, the quick initial peak and rapid decline of brain activity using [^{11}C](*R*)-PK 11195 in some healthy subjects (Fig. 2 in (Kropholler et al., 2005)) looks similar to that in our nonbinders. Although speculative, could [^{11}C](*R*)-PK 11195 have such low specific binding that nonbinders are not as easily identified as with [^{11}C]PBR28? Like other questions of comparison, the answer will likely require side-by-side comparison of the two radioligands in binders and nonbinders.

CONCLUSIONS

Binding of [^{11}C]PBR28 in brain was measured in healthy human subjects with ~90 min of brain imaging combined with serial concentrations of [^{11}C]PBR28 in arterial plasma. Binding in human brain was about 1/20th of that in rhesus monkey and required a two-tissue compartment model. For unknown reason(s), a small percentage (~14%) of healthy subjects showed no significant binding of [^{11}C]PBR28 in brain.

Supplementary Material

Refer to Web version on PubMed Central for supplementary material.

Acknowledgements

We thank Janet L. Sangare, MS, C-RNP, Alicja Lerner, MD, PhD, and the staff of the PET Department for successful completion of PET scans; PMOD Technologies (Adliswil, Switzerland) for providing its image analysis and modeling software; John L. Musachio, PhD and Emmanuelle Briard, PhD for contributions to the preparation of the exploratory IND; Ed Tuan, BS, for assisting with the radiometabolite analysis, Kohji Abe, PhD for analyzing data; and Amira K Brown, PhD for providing results of whole body imaging.

Financial support

This research was supported by the Intramural Program of NIMH (project #Z01-MH-002795-04).

Appendix

MSC is calculated by the following formula,

$$MSC = \ln\left(\frac{\sum_{i=1}^{n} w_i\left(Y_{obs_i} - \bar{Y}_{obs}\right)^2}{\sum_{i=1}^{n} w_i\left(Y_{obs_i} - Y_{cal_i}\right)^2}\right) - 2p/n$$

where n is the number of data points, w_i is the weights applied to the points, p is the number of parameters, Y_{cali} is the value calculated by a model and Y_{obsi} are the observed data in an experiment.

References

Akaike H. A new look at the statistical model identification. IEEE Trans. Automat. Contr 1974;AC19:716–723.

Bevington, PR.; Robinson, DK. Data reduction and error analysis for the physical sciences. McGraw-Hill; New York: 2003.

Briard E, Zoghbi SS, Imaizumi M, Gourley JP, Shetty HU, Hong J, Cropley V, Fujita M, Innis RB, Pike VW. Synthesis and evaluation in monkey of two sensitive ^{11}C-labeled aryloxyanilide ligands for imaging brain peripheral benzodiazepine receptors *in vivo*. J. Med. Chem. in press

Brown AK, Fujita M, Fujimura Y, Liow J-S, Stabin M, Ryu YH, Imaizumi M, Hong J, Pike VW, Innis RB. Radiation dosimetry and biodistribution in monkey and man of ^{11}C-PBR28, a PET radioligand to image inflammation. J. Nucl. Med. In press

Burger C, Mikolajczyk K, Grodzki M, Rudnicki P, Szabatin M, Buck A. JAVA tools quantitative post-processing of brain PET data. J. Nucl. Med 1998;39:277.

Cagnin A, Myers R, Gunn RN, Lawrence AD, Stevens T, Kreutzberg GW, Jones T, Banati RB. In vivo visualization of activated glia by [^{11}C](R)-PK11195-PET following herpes encephalitis reveals projected neuronal damage beyond the primary focal lesion. Brain 2001;124:2014–2027. [PubMed: 11571219]

Carson, RE. Parameter estimation in positron emission tomography. In: Phelps, ME.; Mazziotta, JC.; Schelbert, HR., editors. Positron Emission Tomography and Autoradiography: Principles and Applications for the Brain and Heart. Raven Press; New York: 1986. p. 347-390.

Carson RE, Channing MA, Blasberg RG, Dunn BB, Cohen RM, Rice KC, Herscovitch P. Comparison of bolus and infusion methods for receptor quantitation: applications to [^{18}F]cyclofoxy and positron emission tomography. J. Cereb. Blood Flow Metab 1993;13:24–42. [PubMed: 8380178]

Cymerman U, Pazos A, Palacios JM. Evidence for species differences in ‘peripheral’ benzodiazepine receptors: an autoradiographic study. Neurosci. Lett 1986;66:153–158. [PubMed: 3014385]

Doble A, Malgouris C, Daniel M, Daniel N, Imbault F, Basbaum A, Uzan A, Gueremy C, Le Fur G. Labelling of peripheral-type benzodiazepine binding sites in human brain with [^{3}H]PK 11195: anatomical and subcellular distribution. Brain Res. Bull 1987;18:49–61. [PubMed: 3030512]

Fujimura Y, Ikoma Y, Yasuno F, Suhara T, Ota M, Matsumoto R, Nozaki S, Takano A, Kosaka J, Zhang MR, Nakao R, Suzuki K, Kato N, Ito H. Quantitative analyses of ^{18}F-FEDAA1106 binding to peripheral benzodiazepine receptors in living human brain. J. Nucl. Med 2006;47:43–50. [PubMed: 16391186]

Hawkins RA, Phelps ME, Huang S-C. Effects of temporal sampling, glucose metabolic rates, and disruptions of the blood-brain barrier on the FDG model with and without a vascular compartment: studies in human brain tumors with PET. J. Cereb. Blood Flow Metab 1986;6:170–183. [PubMed: 3485641]

Ikoma Y, Yasuno F, Ito H, Suhara T, Ota M, Toyama H, Fujimura Y, Takano A, Maeda J, Zhang MR, Nakao R, Suzuki K. Quantitative analysis for estimating binding potential of the peripheral benzodiazepine receptor with [^{11}C]DAA1106. J. Cereb. Blood Flow Metab 2007;27:173–184. [PubMed: 16685259]

Imaizumi M, Briard E, Zoghbi SS, Gourley JP, Hong J, Fujimura Y, Pike VW, Innis RB, Fujita M. Brain and whole-body imaging in nonhuman primates of [^{11}C]PBR28, a promising PET radioligand for peripheral benzodiazepine receptors. NeuroImage. In press

Imaizumi M, Briard E, Zoghbi SS, Gourley JP, Hong J, Musachio JL, Gladding R, Pike VW, Innis RB, Fujita M. Kinetic evaluation in nonhuman primates of two new PET ligands for peripheral benzodiazepine receptors in brain. Synapse 2007a;61:595–605. [PubMed: 17455247]

Imaizumi M, Kim H-J, Zoghbi SS, Briard E, Hong J, Musachio JL, Ruetzler C, Chuang D-M, Pike VW, Innis RB, M F. PET imaging with [^{11}C]PBR28 can localize and quantify upregulated peripheral benzodiazepine receptors associated with cerebral ischemia in rat. Neurosci. Lett 2007b;411:200–205. [PubMed: 17127001]

Innis RB, Cunningham VJ, Delforge J, Fujita M, Gjedde A, Gunn RN, Holden J, Houle S, Huang S-C, Ichise M, Iida H, Ito H, Kimura Y, Koeppe RA, Knudsen GM, Knuuti J, Lammertsma AA, Laruelle M, Logan J, Maguire RP, Mintun MA, Morris ED, Parsey R, Price JC, Slifstein M, Sossi V, Suhara T, Votaw JR, Wong DF, Carson RE. Consensus nomenclature for *in vivo* imaging of reversibly binding radioligands. J. Cereb. Blood Flow Metab 2007;27:1533–1539. [PubMed: 17519979]

Kropholler MA, Boellaard R, Schuitemaker A, Folkersma H, van Berckel BN, Lammertsma AA. Evaluation of reference tissue models for the analysis of [^{11}C](*R*)-PK11195 studies. J. Cereb. Blood Flow Metab 2006;26:1431–1441. [PubMed: 16511500]

Kropholler MA, Boellaard R, Schuitemaker A, van Berckel BN, Luurtsema G, Windhorst AD, Lammertsma AA. Development of a tracer kinetic plasma input model for (*R*)-[^{11}C]PK11195 brain studies. J. Cereb. Blood Flow Metab 2005;25:842–851. [PubMed: 15744248]

Kurumaji A, Nomoto H, Yoshikawa T, Okubo Y, Toru M. An association study between two missense variations of the benzodiazepine receptor (peripheral) gene and schizophrenia in a Japanese sample. J Neural Transm 2000;107:491–500. [PubMed: 11215759]

Maeda J, Suhara T, Zhang MR, Okauchi T, Yasuno F, Ikoma Y, Inaji M, Nagai Y, Takano A, Obayashi S, Suzuki K. Novel peripheral benzodiazepine receptor ligand [^{11}C]DAA1106 for PET: an imaging tool for glial cells in the brain. Synapse 2004;52:283–291. [PubMed: 15103694]

Okuyama S, Chaki S, Yoshikawa R, Ogawa S, Suzuki Y, Okubo T, Nakazato A, Nagamine M, Tomisawa K. Neuropharmacological profile of peripheral benzodiazepine receptor agonists, DAA1097 and DAA1106. Life Sci 1999;64:1455–1464. [PubMed: 10321725]

Papadopoulos V, Lecanu L, Brown RC, Han Z, Yao ZX. Peripheral-type benzodiazepine receptor in neurosteroid biosynthesis, neuropathology and neurological disorders. Neurosci 2006;138:749–756.

Pappata S, Cornu P, Samson Y, Prenant C, Benavides J, Scatton B, Crouzel C, Hauw JJ, Syrota A. PET study of carbon-11-PK 11195 binding to peripheral type benzodiazepine sites in glioblastoma: a case report. J. Nucl. Med 1991;32:1608–1610. [PubMed: 1651383]

Pazos A, Cymerman U, Probst A, Palacios JM. 'Peripheral' benzodiazepine binding sites in human brain and kidney: autoradiographic studies. Neurosci. Lett 1986;66:147–152. [PubMed: 3725180]

Venneti S, Lopresti BJ, Wang G, Slagel SL, Mason NS, Mathis CA, Fischer ML, Larsen NJ, Mortimer AD, Hastings TG, Smith AD, Zigmond MJ, Suhara T, Higuchi M, Wiley CA. A comparison of the

high-affinity peripheral benzodiazepine receptor ligands DAA1106 and (R)-PK11195 in rat models of neuroinflammation: implications for PET imaging of microglial activation. J. Neurochem 2007a; 102:2118–2131. [PubMed: 17555551]

Venneti S, Lopresti BJ, Wiley CA. The peripheral benzodiazepine receptor (Translocator protein 18kDa) in microglia: from pathology to imaging. Progress in Neurobiology 2006;80:308–322. [PubMed: 17156911]

Venneti S, Wagner AK, Wang G, Slagel SL, Chen X, Lopresti BJ, Mathis CA, Wiley CA. The high affinity peripheral benzodiazepine receptor ligand DAA1106 binds specifically to microglia in a rat model of traumatic brain injury: implications for PET imaging. Exp Neurol 2007b;207:118–127. [PubMed: 17658516]

Zavala F, Haumont J, Lenfant M. Interaction of benzodiazepines with mouse macrophages. Eur. J. Pharmacol 1984;106:561–566. [PubMed: 6151510]

Zhang MR, Kida T, Noguchi J, Furutsuka K, Maeda J, Suhara T, Suzuki K. [^{11}C]DAA1106: radiosynthesis and in vivo binding to peripheral benzodiazepine receptors in mouse brain. Nucl. Med. Biol 2003;30:513–519. [PubMed: 12831989]

Zhang MR, Maeda J, Ogawa M, Noguchi J, Ito T, Yoshida Y, Okauchi T, Obayashi S, Suhara T, Suzuki K. Development of a new radioligand, N-(5-fluoro-2-phenoxyphenyl)-N-(2-[18F]fluoroethyl-5-methoxybenzyl)acetami de, for pet imaging of peripheral benzodiazepine receptor in primate brain. J. Med. Chem 2004;47:2228–2235. [PubMed: 15084121]

Zoghbi SS, Shetty HU, Ichise M, Fujita M, Imaizumi M, Liow JS, Shah J, Musachio JL, Pike VW, Innis RB. PET imaging of the dopamine transporter with ^{18}F-FECNT: a polar radiometabolite confounds brain radioligand measurements. J. Nucl. Med 2006;47:520–527. [PubMed: 16513622]

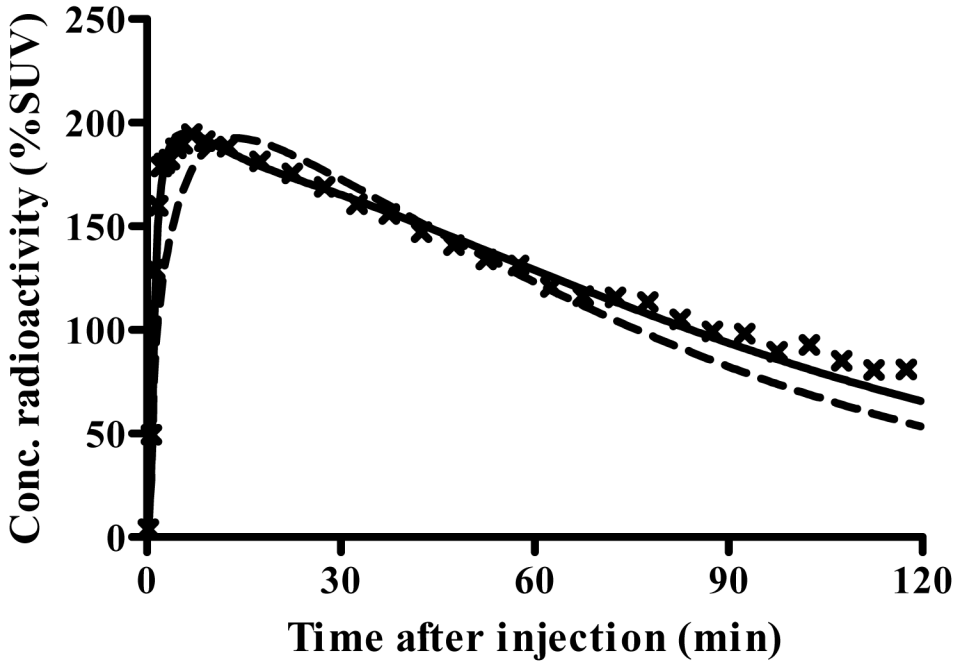

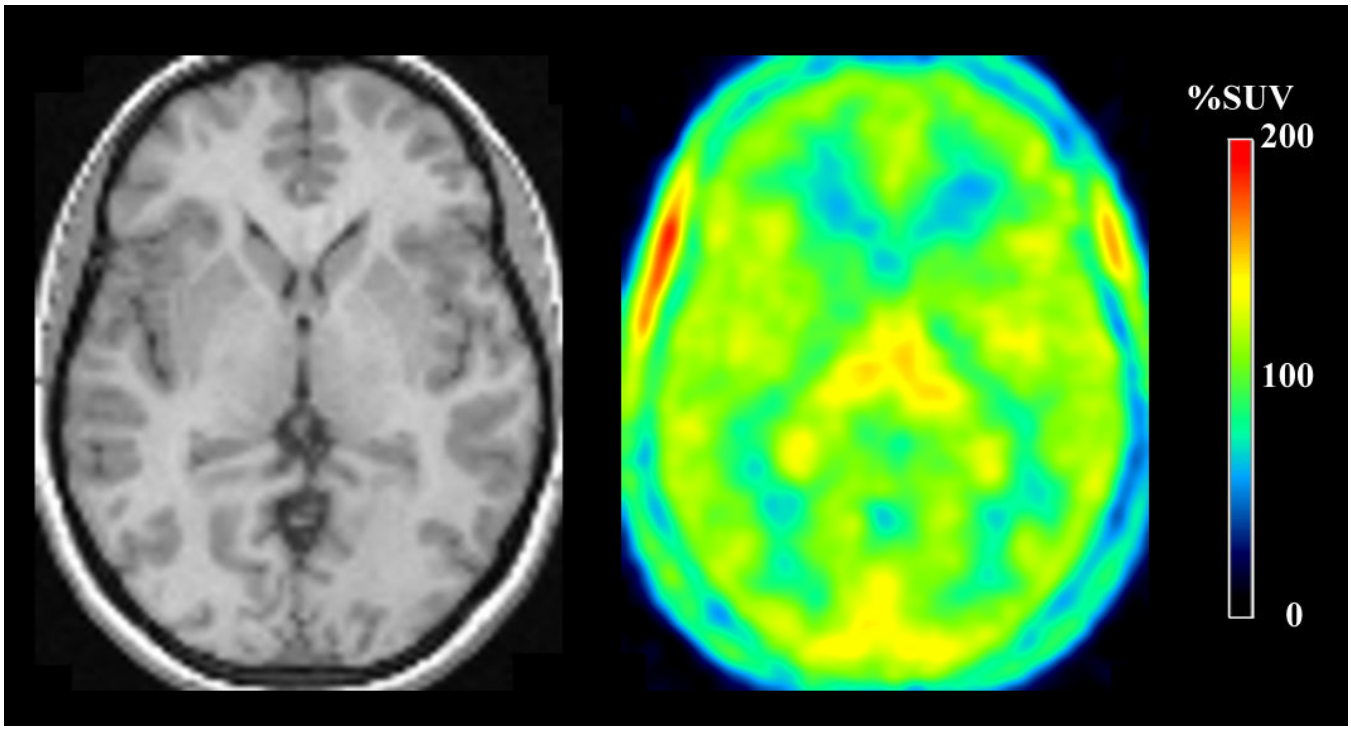

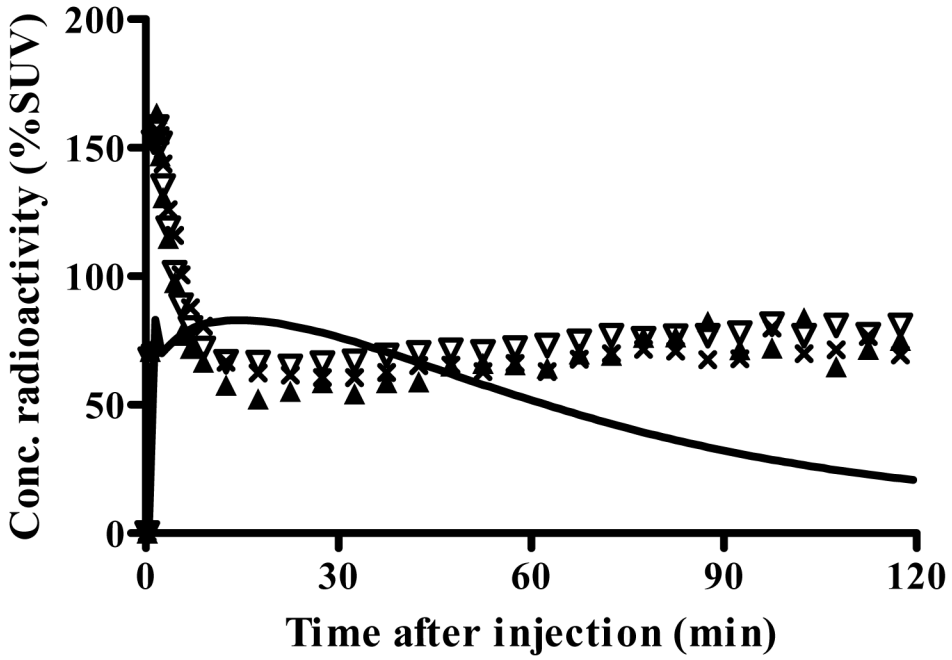

Fig. 1.

Time course of radioactivity and images of its distribution in brain after injection of [^{11}C] PBR28. **A)** Concentrations (×) of radioactivity in thalamus of a typical healthy subject - namely, one who showed binding of the radioligand. The measured data were fitted with one- and two-tissue compartment models with no constraint. The two-tissue compartment model (▬) more closely followed the measured values than did the one-compartment model (▬ ▬ ▬). The constrained two-tissue compartment model with a fixed value of K_1/k_2 (not plotted) was visually indistinguishable from the unconstrained two-compartment model. **B**) The transverse PET image (right) of this typical healthy subject was created by averaging all frames and scaled using %SUV. The coregistered MRI (left) of this subject identifies that the PET image was obtained at the level of the thalamus. **C**) Concentrations of radioactivity in thalamus (×), caudate (▲), and parietal cortex (▽) in an atypical human subjects - i.e., one who appeared to have no binding of the radioligand. The one-compartment fitting (solid line) converged but with large deviations from the observed data, and two-compartmental fitting (not plotted) did not converge.

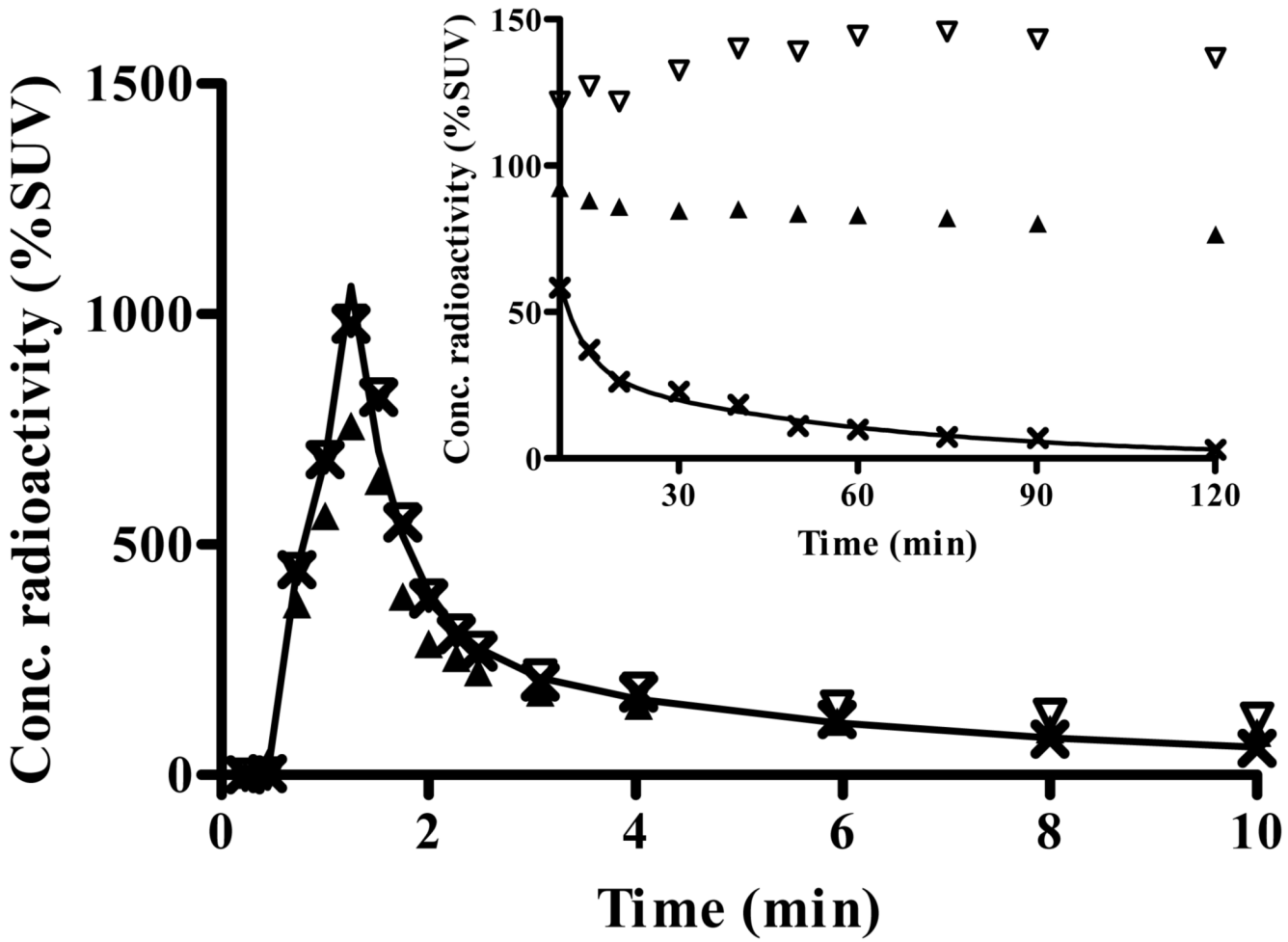

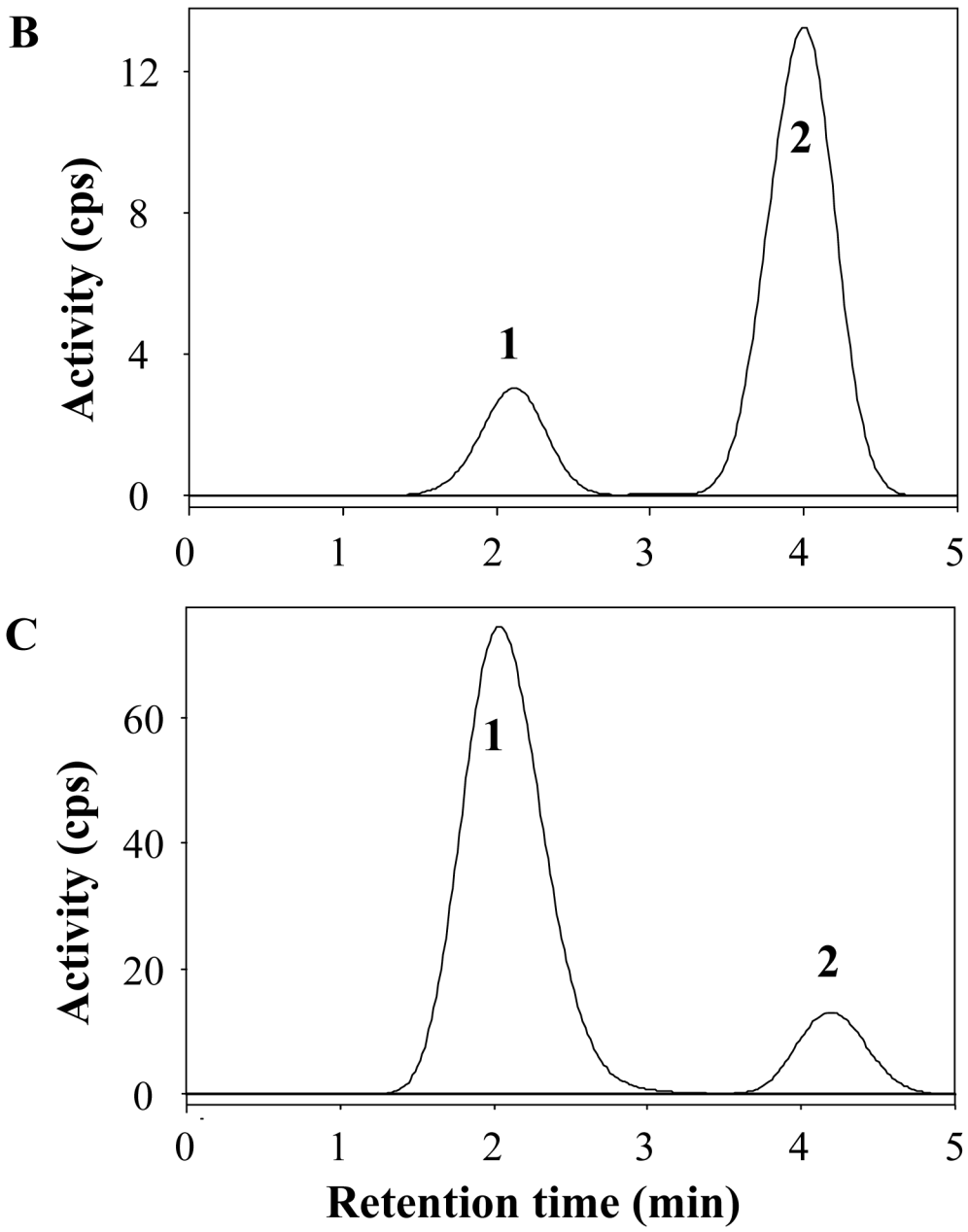

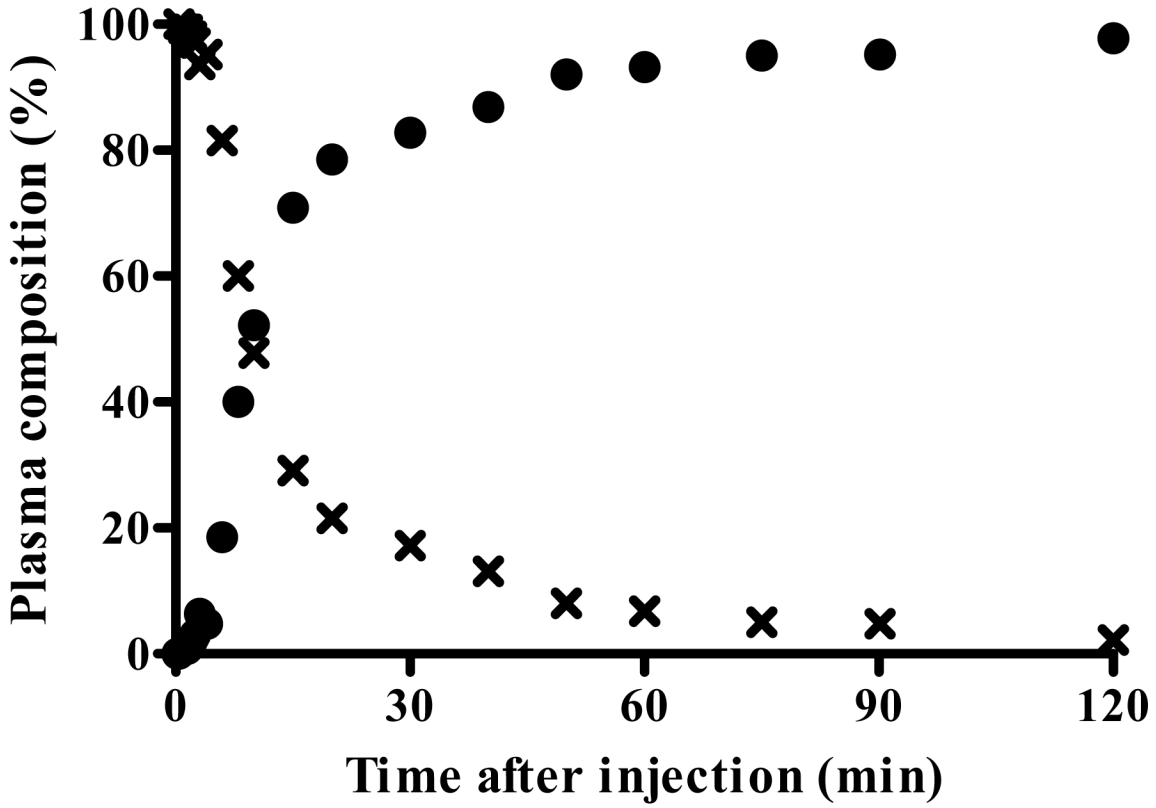

Fig. 2.

Concentration of radioactivity in plasma of the typical healthy subject shown in Fig. 1A and 1B. **A)** Concentrations are plotted for unchanged parent radioligand [^{11}C]PBR28 (×), total radioactivity in blood (▲), and total radioactivity in plasma (▽). The time course of [^{11}C] PBR28 was fitted to a tri-exponential curve (▬). Radiochromatograms of activity extracted from plasma at 6 (**B**) and 40 (**C**) min after injection of [^{11}C]PBR28. Peak 2 was confirmed to be [^{11}C]PBR28 based on HPLC co-elution with nonradioactive PBR28. Peak 1 was a radiometabolite with lipophilicity lower than that of [^{11}C]PBR28. **D**) The percentage composition of plasma radioactivity over time is shown for [^{11}C]PBR28 (×) and the radiometabolite (●).

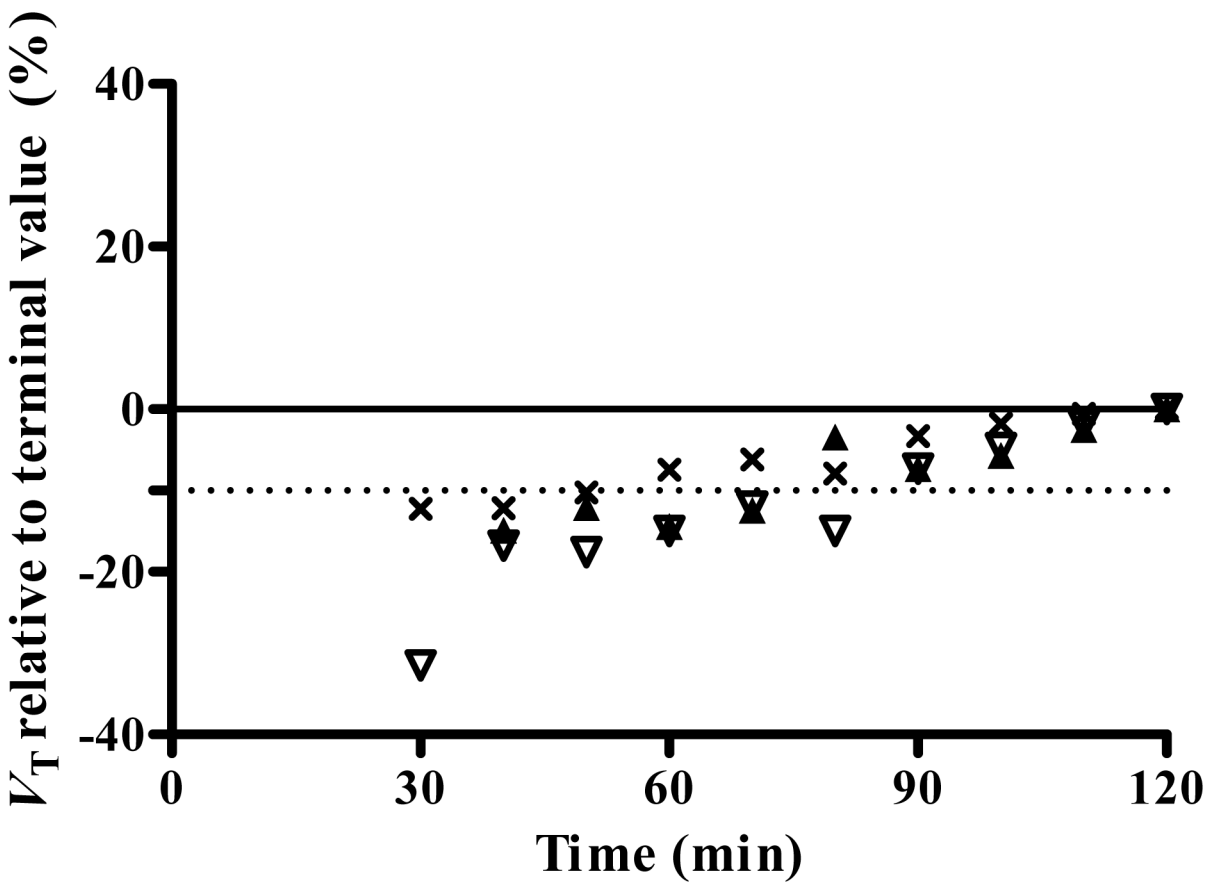

Fig. 3.

Value of distribution volume as a function of duration for image acquisition. V_T was calculated for thalamus (×), caudate (▲), and parietal cortex (▽) using an unconstrained two-tissue compartment model. Scans were analyzed using brain data from time 0 to the specified time on *x*-axis. V_T was expressed as a percentage of terminal value - *i.e.*, V_T calculated from the entire 120-min data set. Imaging for the initial 90 min provided V_T within 10% (dashed line) of that obtained with the full length data.

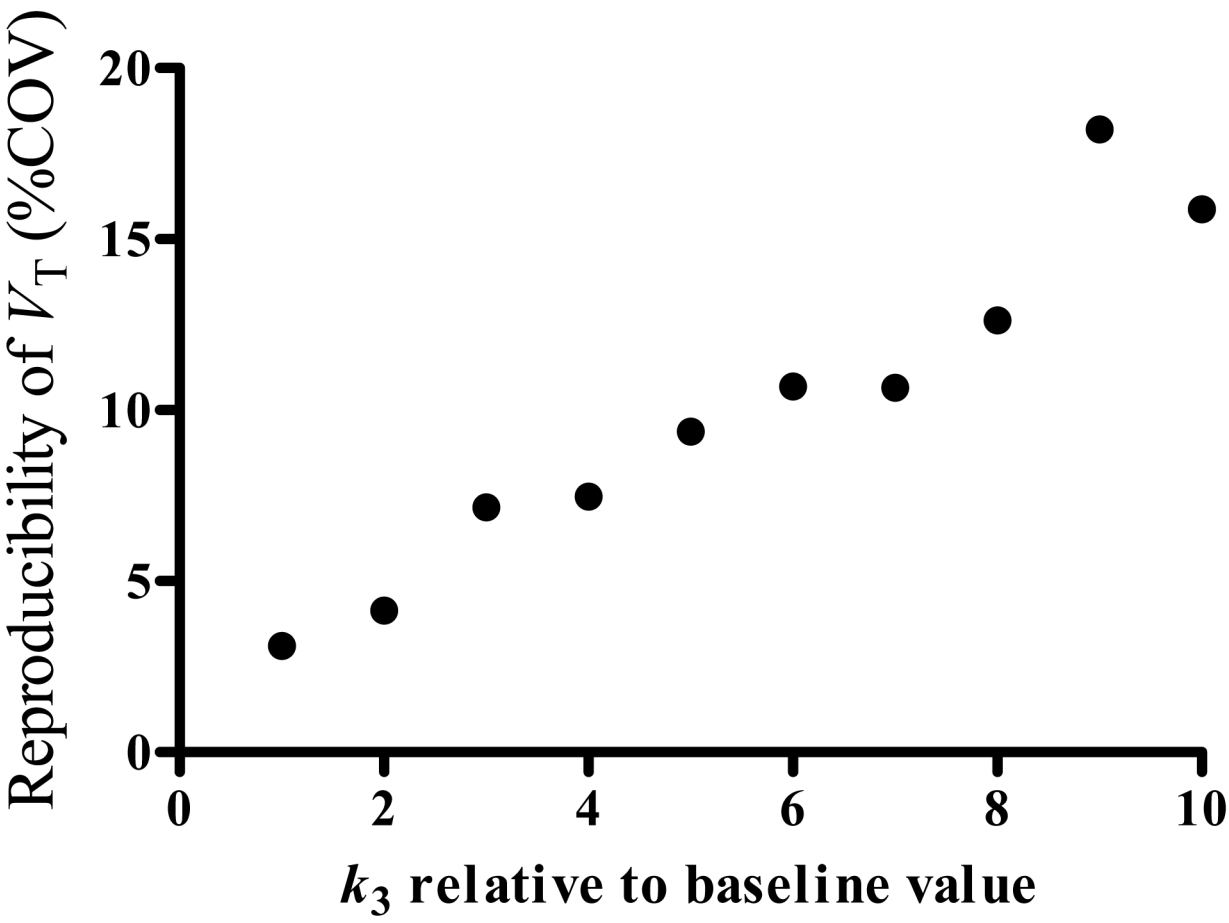

Fig. 4.

Reproducibility of distribution volume estimation as a function of receptor density, as simulated by increasing the value of k_3. Simulations were performed by using average rate constants obtained in thalamus (K_1 = 0.12 mL • cm^{-3} · min^{-1}, k_2 = 0.11 min^{-1}, k_3 = 0.069 min^{-1}, and k_4 = 0.023 min^{-1}) and average input function, and by increasing k_3 up to 10 times of its baseline value. The increases caused poorer reproducibility (i.e., larger %COV), but the %COV was still less than 10% for a five-fold increase in k_3.

Table 1

Kinetic rate constants estimated with unconstrained two-comparment model

Region	K_1 (mL • cm^{-3} • min^{-1})	k_2 (min^{-1})	k_3 (min^{-1})	k_4 (min^{-1})	BP_{ND}	V_T (mL • cm^{-3})	AIC	MSC
Thalamus	0.13 ± 0.043 (3.1 ± 0.8)	0.13 ± 0.033 (9.4 ± 2.2)	0.085 ± 0.028 (10.1 ± 2.1)	0.024 ± 0.0058 (6.2 ± 1.9)	3.5 ± 0.7 (7.8 ± 2.0)	4.6 ± 1.6 (2.5 ± 0.9)	92 ± 72	4.3 ± 0.4
Caudate	0.11 ± 0.036 (3.9 ± 1.0)	0.10 ± 0.027 (11.0 ± 3.4)	0.045 ± 0.019 (18.7 ± 4.9)	0.023 ± 0.0089 (18.6 ± 12.4)	2.0 ± 0.5 (13.9 ± 8.8)	3.3 ± 1.0 (7.5 ± 8.5)	118 ± 71	3.7 ± 0.4
Cerebellum	0.14 ± 0.046 (3.4 ± 1.5)	0.13 ± 0.037 (9.0 ± 2.2)	0.069 ± 0.028 (11.4 ± 2.4)	0.027 ± 0.0069 (7.6 ± 3.5)	2.5 ± 0.6 (7.8 ± 1.8)	4.1 ± 1.3 (2.6 ± 1.4)	100 ± 70	4.5 ± 0.5
Pons	0.10 ± 0.036 (3.7 ± 1.1)	0.13 ± 0.036 (10.6 ± 2.2)	0.078 ± 0.021 (10.7 ± 2.3)	0.018 ± 0.0042 (8.1 ± 2.3)	4.5 ± 0.9 (8.0 ± 1.5)	4.5 ± 1.6 (4.0 ± 1.2)	92 ± 69	3.5 ± 0.3
Parietal Cx.	0.12 ± 0.037 (2.7 ± 1.7)	0.10 ± 0.027 (8.0 ± 4.1)	0.050 ± 0.025 (12.4 ± 2.8)	0.023 ± 0.0082 (10.4 ± 4.8)	2.1 ± 0.5 (8.2 ± 3.3)	3.9 ± 1.1 (3.7 ± 2.4)	90 ± 68	4.6 ± 0.4

Numbers in parentheses represent identifiability (%).

AIC: Akaike Information Criterion

MSC: Model Selection Criterion

Table 2

Kinetic rate constants estimated with one-comparment model

Region	K_1 (mL • cm^{-3} • min^{-1})	k_2 (min^{-1})	V_T (mL • cm^{-3})	AIC	MSC
Thalamus	0.081 ± 0.024 (3.5 ± 0.6)	0.023 ± 0.004 (6.9 ± 1.0)	3.6 ± 1.3 (4.5 ± 0.7)	187 ± 90	1.5 ± 0.3
Caudate	0.078 ± 0.022 (4.1 ± 0.8)	0.034 ± 0.008 (6.9 ± 0.9)	2.4 ± 0.8 (4.1 ± 0.5)	183 ± 69	1.7 ± 0.3
Cerebellum	0.092 ± 0.024 (3.8 ± 0.6)	0.030 ± 0.004 (6.7 ± 1.3)	3.2 ± 1.1 (4.1 ± 0.8)	192 ± 73	1.7 ± 0.4
Pons	0.062 ± 0.019 (3.9 ± 0.7)	0.019 ± 0.003 (8.4 ± 1.3)	3.3 ± 1.2 (5.7 ± 0.9)	181 ± 70	0.8 ± 0.4
Parietal Cx.	0.083 ± 0.023 (3.6 ± 0.8)	0.029 ± 0.005 (6.3 ± 1.1)	2.9 ± 1.0 (3.9 ± 0.7)	182 ± 71	1.8 ± 0.4

Numbers in parentheses represent identifiability (%).

AIC: Akaike Information Criterion

MSC: Model Selection Criterion